Reduced electron-phonon relaxation rates in quantum-box systems: Theoretical analysis

H. Benisty
Laboratoire Central de Recherches, Thomson-CSF, F-91404 Orsay Cedex, France
(Received 11 October 1994; revised manuscript received 19 December 1994)

Reasons for the reduced electron-phonon relaxation arising in the conduction band of zero-dimensional quantum-box (QB) systems when level separation is of the order of 1 meV or larger are explained. Relaxation rates are calculated using approximations of the electron-phonon interaction matrix element between two given levels. A threshold QB energy-level separation and a threshld QB size for reduced relaxation are then deduced. To deal with the multilevel situation encountered in flat square boxes with two dimensions much larger than the third one, it is shown that the energy-independent density of states in a given subband translates into a Poissonian distribution of the level separation. This statistical approach is developed to predict the occurrence of relaxation bottlenecks along a cascade of levels in intra- and intersubband transitions cases.

I. INTRODUCTION

Semiconductor quantum boxes (QB's) have been described as promising for applications in optical and optoelectronic devices owing to their quantized atomlike levels.[1–3] Although their discrete levels are undoubtedly advantageous for optical purposes, they might considerably hinder carrier relaxation for level separations ΔE as small as ~ 1 meV.[4] This is a major issue since energy separations $\Delta E \sim 25$ meV are required to take advantage of discrete levels at room temperature.[3] This issue was addressed in Ref. 5, suggesting that reduced relaxation could provide an intrinsic mechanism for the poor luminescence yields of boxes as large as 150×150 nm^2 compared to the 30×30 nm^2 needed to reach $\Delta E \sim 25$ meV between box levels in the same system. Owing to continuous progresses in nanostructure fabrication and increased elimination of extrinsic nonradiative recombination mechanisms, a more complex picture has emerged. On the one hand, some experiments have clearly pointed out the presence of ordinary luminescence from excited levels in a single-box system, a clear signature of reduced relaxation.[6,7] On the other hand, some alternative relaxation mechanisms have been proposed in specific situations: interaction with specific phonons,[8] plasma-assisted relaxation,[9] electron-hole interactions.[10] This last channel is difficult to evaluate quantitatively owing to the complex valence-band structure. In this paper, we shall therefore focus on hole-free situations, a situation which makes relaxation through acoustic-phonon relaxation the predominant relaxation channel.

Intraband radiative transitions (e.g., intersubband transitions) are now a growing field of interest where the valence band, being filled, cannot help electron relaxation. Electrons are just neutralized by dopants, whose energy levels do not allow the few-meV relaxation needed among quantum-box levels of interest here. Therefore relaxation in this situation clearly relies on acoustic phonons only.

It is thus attempted here to describe properly, and with some generality, reduced electron relaxation among a plurality of box levels, for which only examples had been treated in Ref. 5. The aim of this paper is twofold: (i) to detail and clarify the origin of the reduced electron–acoustic-phonon interaction, giving analytical expressions appropriate to electrons' relaxation rates between QB states; (ii) to extend the analysis of the model multilevel box of Ref. 5 using a statistical approach instead of a single box to predict on a more general basis the appearance of bottlenecks on the relaxation path of electrons. As will be discussed elsewhere[11] such relaxation bottlenecks can greatly improve the efficiency of important optoelectronic systems (e.g., infrared) relying on intraband transitions (e.g., intersubband transitions).

The organization is as follows. In the next section (Sec. II), basic assumptions on box dimensions and materials allowing one to focus on electron–LA-phonon relaxation are presented; reduced relaxation is then outlined from energy and momentum conservation rules. In Sec. III, electron-phonon scattering rates between box levels are calculated. Section IV is devoted to a statistical approach based on the distribution of QB level separations; appearance of relaxation bottlenecks is predicted and their specific distribution law discussed; application to intrasubband and intersubband transition cases is finally presented. Mathematical aspects of the statistical approach are to be found in the Appendixes.

II. BASIC ASSUMPTIONS

A. Carriers and phonons

We will in the following concentrate on electron relaxation, as hole levels, due to their typically ~ 10 times heavier mass, have correspondingly smaller energy separations than electron levels for given box dimensions. As outlined above, we consider the valence band to be filled, the electron population being controlled through doping, a common situation in intersubband-transition-based devices.

In a usual two-dimensional (2D) system, excited electrons lose their energy to both optical and acoustic pho-

nons.[4,12,13] The former are very efficient in polar compounds of interest here through the dipole-coupled LO mode. However, these branches are dispersionless near zone center, which implies a separation ΔE matching the optical phonon energy $E_{\rm opt}$, about 30 meV in typical materials. The same remark holds for the possible excitation of neutral donors to an excited level: the first excited level for most donors lies at a well-defined energetic height, typically $\sim$20 meV, above the ground state.

Therefore, already for large box sizes ($\sim$100 nm diameter) and $\Delta E \sim 1-5$ meV $\ll E_{\rm opt}$, relaxation throughout the numerous levels towards the ground state by LO-phonon emission might be somewhat diminished, due to the difficulty of finding an energy-matched final level. We will, however, concentrate here on the last steps of relaxation towards the ground state, within an energy range of $E_{\rm opt}$, which then relies on acoustic-phonon emission only.

For narrower confinements (<50 nm) and larger separations, the probability that ΔE matches $E_{\rm opt}$ surely vanishes and carriers above $E_{\rm opt}$ also have to relax through acoustic phonons. Finally, in the low-temperature limit, the two-phonon processes involving acoustic phonons (e.g., LO+LA, etc.), whose energy requirements are less stringent, are also very weak, leaving acoustic phonons as the only relaxation channel.

For the sake of simplicity and since we study the Γ valley of a cubic crystal, we approximate the various acoustic-phonon branches by a single isotropic branch, using a single averaged sound velocity c_s. Also, piezoelectric scattering is ignored because it is known to be only $\sim$10% of deformation potential scattering.[14]

B. The quantum-box system

We consider a system consisting of a quantum well of lower-band-gap material of thickness L_z($\sim$2–35 nm) epitaxially grown in the z direction between layers of higher-band-gap material (a type-I quantum well is assumed). For typical III-V systems with low effective mass m^*, such as GaAs/$Ga_{1-x}Al_xAs$ and $In_{0.53}Ga_{0.47}As$/InP, this leads to $\sim$0.1–1 eV barrier heights at Γ-band edges. The nth envelope wave function ψ_z in the z direction has the well-known $\sin(k_z z)$ shape in the well with $k_z \sim n\pi/L_z$, k_z being the solution of an implicit equation,[15] and decaying exponentially in the barriers. The corresponding energy is written

$$E = E_{x,y} + E_n = E_{x,y} + \frac{\hbar^2 k_z^2}{2m^*} . \tag{1}$$

If such a layer is patterned in lateral x,y directions with dimensions $L_x, L_y \gg L_z$, the infinite-barrier approximation can be applied to the wave function in the x,y directions, yielding

$$\psi = \psi_x \psi_y \psi_z = (L_x L_y)^{-1/2} \sin(k_x x)\sin(k_y y)\psi_z \tag{2}$$

with $k_x = l\pi/L_x$, $k_y = m\pi/L_y$. The energy is then

$$E_{l,m,n} = \frac{\hbar^2\pi^2}{2m^*}\left[\frac{l^2}{L_x^2} + \frac{m^2}{L_y^2}\right] + \frac{\hbar^2 k_z^2}{2m^*} . \tag{3}$$

We shall now explain the basis of the reduced relaxation between such levels below a critical size, focusing on the square box ($L_x = L_y$) z ground state ($n=1$), and infinite-well approximation ($k_z = \pi/L_z$).

C. Basic reason for reduced relaxation

The basic reason for vanishing relaxation when L_x is reduced is the impossibility of satisfying simultaneously energy and momentum conservation during an electron–acoustic-phonon scattering event. We will first evidence a maximum, size-independent, level separation $(\Delta E)_{\rm max}$ for allowed scattering. Then, using the confinement energy, we translate $(\Delta E)_{\rm max}$ into a minimum threshold box size.

We consider the energy range $E_{1,1,n=1} < E_{l,m,1} \ll E_{1,1,n=2}$, to ensure $E_{x,y} \ll E_z$ and $k_\parallel \ll k_z$. Let us denote the phonon wave vector $\mathbf{q}$ and initial and final electron levels $|i\rangle$ and $|f\rangle$. Momentum conservation takes place through interlevel matrix elements $\langle i|e^{i\mathbf{q}\cdot\mathbf{r}}|f\rangle$ of the form[4]

$$\int e^{i(\mathbf{k}_\parallel + \mathbf{k}_z)_i \cdot \mathbf{r}} e^{i\mathbf{q}\cdot\mathbf{r}} e^{i(\mathbf{k}_\parallel + \mathbf{k}_z)_f \cdot \mathbf{r}} .$$

This tells us that for phonons leading to significant scattering rates, $q_\parallel$ is at most $(k_\parallel)_i + (k_\parallel)_f \ll 2\pi/L_z$. For q_z, the localized character of the $n=1$ level translates into a momentum distributed from 0 up to $2\pi/L_z$, but rapidly vanishing above this value. As $q_\parallel \ll 2\pi/L_z$, if q exceeds $q_{\rm max} \approx 2\pi/L_z$, the matrix element and the scattering probability vanish. The maximum phonon energy $E^{\rm crit}$ associated with $q_{\rm max}$ is $E^{\rm crit} = \hbar c_s (k_{\rm ph})_{\rm max} \sim h c_s / L_z$, irrespective of L_x. For typical materials and $L_z = 100$ Å, $E^{\rm crit}$ is quite low, of the order of 1 or a few meV. Hence, due to energy conservation, a scattering event involving $\Delta E > E^{\rm crit} \sim 1$ meV becomes extremely unlikely.

Turning to the effect of box size, the lateral confinement energy $E_{\rm conf} = \hbar^2\pi^2/(2m^* L_x^2)$ gives a convenient order of magnitude of a typical separation ΔE between two neighboring levels $E_{l,m,1}$ and $E_{l',m',1}$, albeit underestimated (see Sec. IV). Writing $E_{\rm conf} = E^{\rm crit}$ gives

$$L_x^{\rm crit} \approx \left[\frac{\pi\hbar^2 L_z}{4m^* c_s}\right]^{1/2} . \tag{4}$$

It is of the order of 1000 Å, a large value compared to the required size to obtain room-temperature 3D quantum effects ($\approx$200 Å), due to the rather low value of $E^{\rm crit} \sim 1$ meV. For smaller sizes, relaxation will be strongly reduced for most significant electronic transitions.[4] We now calculate in detail the matrix element in $\mathbf{k}$ space.

III. ELECTRON-PHONON RELAXATION RATES BETWEEN LEVELS OF A BOX

The transition rate w_{if} between two lateral levels $i \equiv (l,m), f \equiv (l',m')$ of the same subband n, separated by $E_{\rm if}$, due to acoustic phonons can be written from the Fermi golden rule as a sum on phonon modes:[4]

$$w_{if}=\frac{1}{\tau_{i\to f}}=\frac{2\pi}{\hbar}\sum_{\mathbf{q}}E_q\frac{D^2}{2\rho c_s^2\Omega}|\langle\psi_f|e^{\pm i\mathbf{q}\cdot\mathbf{r}}|\psi_i\rangle|^2 \times\delta(E_f-E_i\pm E_q)\left[n_B(E_q)+\begin{Bmatrix}1\\0\end{Bmatrix}\right], \tag{5}$$

where D, the deformation potential, gives the strength of electron–acoustic-phonon coupling, E_q is the phonon energy, ρ is the crystal density, and Ω is a normalization volume. The δ function accounts for energy conservation. The upper signs hold for phonon emission and the lower for absorption; $n_B(E_q)$ is the Bose-Einstein phonon occupancy number and we will note $n_B'(E_q)=n_B(E_q)+1$ for phonon emission. Bulk acoustic phonons are a very good approximation because their reflection coefficients at layer interfaces are quite low.

The squared matrix element, denoted $M(\mathbf{q})$, reflects momentum conservation. It is of order unity if there is a noticeable $\mathbf{q}$ Fourier component in $\psi_f^*\psi_i$ and vanishes otherwise. M is separable, that is,

$$M(\mathbf{q})=M_x(q_x)M_y(q_y)M_z(q_z)=M_{\parallel}(\mathbf{q}_{\parallel})M_z(q_z)\ .$$

In the infinite-barrier approximation, the particular form of, say, M_x, between levels l and l' is

$$M(q_x)=\tfrac{1}{4}\left|\sum_{\nu=\pm l\pm l'}s_\nu\frac{\sin[(q_xL_x+\nu\pi)/2]}{(q_xL_x+\nu\pi)/2}\right|^2 \tag{6}$$

with the signs s_ν given in Appendix A, Table II. With finite barriers, namely, for M_z, a small barrier contribution has to be added but the overall behavior, in particular at large q, is unchanged (see Appendix C). M_x is seen to consist of four peaks located at $Q_x=(\pm l\pm l')\pi/L_x$. This recalls the usual $\delta(k_x-k_x'+Q_x)$ selection rule, looking at each level as a sum of $(k_x,-k_x)$ running waves. Each peak has a width $2\pi/L_x$ due to localization. Keeping these modifications in mind, quasiconservation of momentum amounts to selecting the regions where M is ~ 1. As previously, if we restrict ourselves to energies below $E_{112}\equiv E_2$, we have $(k_x,k_y)<k_z$. Then the $\mathbf{q}$ region where $M\sim 1$ is most extended along q_z, reaching about $K_z=3\pi/2L_z$, which is larger than $K_x=(l+l')\pi/L_x$ and $K_y=(m+m')\pi/L_y$ along q_x and q_y. The $M\sim 1$ region is schematized by the dashed ellipsoid in Fig. 1, of width K_x,K_y and of height K_z, ignoring the detailed structure of the peaks at Q_x,Q_y. Notice that K_x grows when going to narrower lateral confinements [from Fig. 1(a) to 1(c)], remaining smaller than K_z, however.

Turning to the energy conservation requirement, the phonon energy is

$$E_{if}=E_i-E_f=\frac{\hbar^2}{2m^*}(k_{\parallel}^2-k_{\parallel}'^2)=\frac{\hbar^2}{2m^*}\pi^2\left[\frac{l^2-l'^2}{L_x^2}+\frac{m^2-m'^2}{L_y^2}\right]. \tag{7}$$

This in turn determines the phonon momentum to be

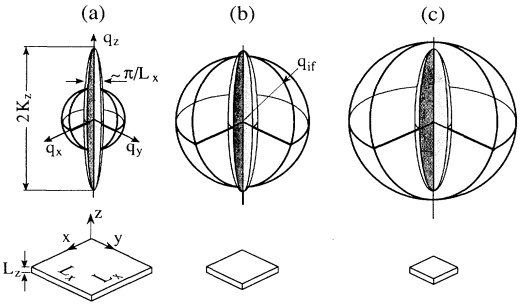

FIG. 1. Picture in the q space of the energy-conserving sphere of radius q_{if} and of the region of momentum conservation $M\sim 1$ for transition between levels of a square box of dimensions $L_x\times L_x\times L_z$. q_{if} scales like L_x^{-2} while the $q_{\parallel}$ extent of M scales like L_x^{-1} and the q_z extent is constant. (a) Large L_x: the $M\sim 1$ region intersects the sphere; (b) smaller L_x: intermediate case, $q_{if}\approx 3\pi/(2L_z)$; (c) small L_x: the sphere intersects only regions of vanishing M.

$\hbar q_{if}=E_{if}/c_s$. Thus we can replace $E_q\delta(E_{if}-E_q)$ by $q\delta(q-q_{if})$. Next, we carry the discrete sum of Eq. (5) into a continuous one in spherical q coordinates using the q solid angle element $d\Omega_q$:

$$w_{if}=\frac{1}{(2\pi)^2}\frac{D^2}{2\rho\hbar c_s^2}\int q^2dq\,d\Omega_q|\langle\psi_f|e^{\pm i\mathbf{q}\cdot\mathbf{r}}|\psi_i\rangle|^2 \times\left[n_B(E_q)+\begin{Bmatrix}1\\0\end{Bmatrix}\right]q\delta(q-q_{if})\ . \tag{8}$$

Using the $\delta(q-q_{if})$ function, we are left with a sum on the sphere of radius q_{if} (see Fig. 1):

$$w_{if}=\frac{1}{(2\pi)^2}\frac{D^2}{2\rho\hbar c_s^2}\left[n_B(E_{if})+\begin{Bmatrix}1\\0\end{Bmatrix}\right]q_{if}^3 \times\int d\Omega_q|\langle\psi_f|e^{\pm i\mathbf{q}\cdot\mathbf{r}}|\psi_i\rangle|^2\ . \tag{9}$$

If this sphere intersects the dashed $M\sim 1$ region, relaxation takes place as in an infinite 2D electron gas (2DEG) [Fig. 1(a)]. When L_x is reduced [Fig. 1(b)], K_x grows according to L_x^{-1} but q_{if} grows faster since $E_{if}\propto L_x^{-2}$. In Fig. 1(b), $q_{if}\approx K_z$ is the threshold situation. On further reducing L_x [Fig. 1(c)], the sphere becomes so large that it does not intersect this region, that is, if $q_{if}>K_z$, M vanishes in Eq. (9) and $w_{\rm if}$ also vanishes. *The threshold for reduced relaxation is thus accounted for by* $q_{if}=K_z$ [Fig. 1(b)] and corresponds to a separation

$$E^{\rm crit}=\hbar c_sK_z=3hc_s/4L_z=3\pi\hbar c_s/2L_z\ ,$$

of the order of 1 meV for usual materials and $L_z=100$ Å. Possible consequences of this value much lower than the thermal energy for the interband properties of quantum boxes have been suggested in Ref. 5.

We now present a useful approximation for w_{if} based on the fact that the main contributions of M to w_{if} are found whenever $M_{\parallel}\sim 1$, whatever the magnitude of M_z. This is straightforward when $q_{if}<K_z$ and $M\sim 1$ regions

do intersect the q_{if} sphere. Then, the intersection region at $q_z \approx \pm q_{if}$ gathers the only noticeable contributions of M to w_{if} in the sum of Eq. (9), around the q_z poles of the q_{if} sphere at values of $\mathbf{q}_\parallel$ where $M_\parallel(\mathbf{q}_\parallel) \sim 1$. More precisely, this corresponds to the vicinity of the peaks of $M_\parallel$ at the quasi-selection-rule values $\mathbf{q}_\parallel = \mathbf{k}_\parallel - \mathbf{k}'_\parallel$, with the $\pm\pi/L_x$ and $\pm\pi/L_y$ spreading around them. The effective area of the intersection region around each pole is defined by

$$S = q_{if}^2 \int d\Omega_q M_\parallel \approx \int d\mathbf{q}_\parallel M_\parallel = \int dq_x dq_y M_x M_y \ . \tag{10}$$

The q_x, q_y sums are calculated in Appendix B using the Bessel-Parseval theorem. The exact result matches the $2\pi/L_x$ intuitive one, except if $l = l'$ or $m = m'$:

$$\int dq_x M_x^{ll'}(q_x) = \frac{\pi}{L_x}(2 + \delta_{ll'}) \ . \tag{11}$$

Replacing x by z and (l, l') by $(1,1)$, this result further justifies the choice of $K_z = 3\pi/2L_z$ as the limit of the $M_z \sim 1$ region because the similar sum of $M_z(q_z)$ from $-\infty$ to $+\infty$ yields $2K_z$.

The approximated value of w_{if} is obtained (i) by converting the surface S into an effective solid angle $\Omega = S/q_{if}^2$ for each pole, i.e., by assuming that the intersection is almost horizontal, and (ii) by replacing correspondingly $M_z(q_z)$ by $M_z(q_{if}) = M_z(-q_{if})$. This is written

$$\begin{aligned} \int d\Omega_q M(\mathbf{q}) &\approx M_z(q_{if}) \int d\Omega_q M_x M_y \\ &\approx 2M_z(q_{if}) \frac{1}{q_{if}^2} \int d\mathbf{q}_\parallel M_\parallel(\mathbf{q}_\parallel) \ , \end{aligned} \tag{12}$$

so that finally the approximation to w_{if} is

$$\begin{aligned} w_{if} &= \frac{D^2}{2\rho\hbar c_s^2} \left[n_B(E_{if}) + \begin{Bmatrix} 1 \\ 0 \end{Bmatrix} \right] \frac{q_{if} M_z(q_{if})}{L_x L_y} (2 + \delta_{ll'} + \delta_{mm'}) \\ &= \frac{D^2}{2\rho\hbar^2 c_s^3} \left[n_B(E_{if}) + \begin{Bmatrix} 1 \\ 0 \end{Bmatrix} \right] \frac{E_{if} M_z(E_{if}/\hbar c_s)}{L_x L_y} (2 + \delta_{ll'} + \delta_{mm'}) \\ &= \frac{\pi^2 D^2}{2\rho m^* c_s^3} \left[n_B(E_{if}) + \begin{Bmatrix} 1 \\ 0 \end{Bmatrix} \right] \frac{M_z(q_{if})}{L_x L_y} \left[\frac{l^2 - l'^2}{L_x^2} + \frac{m^2 - m'^2}{L_y^2} \right] (2 + \delta_{ll'} + \delta_{mm'}) \ , \end{aligned} \tag{13}$$

where the second line makes use of $E_{if} = \hbar c_s q_{if}$ and the last line makes use of Eq. (7).

We claim that this approximation focusing on $M_\parallel \sim 1$ regions is still valid when $q_{if} > K_z$ and $M_z \ll 1$. This is because $M_\parallel(q)$ vanishes much faster than $M_z(q)$ at large q and this is far from being compensated by the larger effective solid angle spanned by M_x, M_z, for example, around the "equator" ($q_z = 0$), compared to the solid angle spanned by $M_\parallel$ around the poles. At large q, the M's are powers of $(1/qL)$, so $L_x, L_y \gg L_z$ ensures a faster decay of $M_\parallel$ compared to M_z.

How strongly relaxation is reduced at large separations is determined by the large-q ($q \gg K_z$) behavior of M_z, a very steep one indeed. Appendix C shows that $M_z(q) \propto 1/q^6$ at large q for $n = 1$, even for the finite well. Assuming low temperatures and $n'_B \approx 1$ (phonon emission), Eq. (13) tells us that w_{if} is proportional to $q_{if}^{-5} L_x^2$ for a square box. *For a given box,* w_{if} is thus proportional to E_{if}^{-5}. *For different boxes* (i.e., different L_x's), q_{if} scales like L_x^{-2}, therefore w_{if} scales like $(L_x^{-2})^{-5}/L_x^2 = L_x^8$, a very steep behavior when L_x is reduced to get additional confinement.

For a finite well, threshold energy and momentum are decreased with respect to an infinite well, as if it had a larger effective thickness. These quantities closely follow the decrease of k_z below its π/L_z value for infinite barriers. As the large-q behavior of M_z remains $M_z(q) \propto q^{-6}$, the overall behavior is unchanged and only the threshold lateral size for reduced relaxation is displaced toward still larger values. Another way to describe this result is to remark that the effect of well finiteness is to smooth the wave function, thereby diminishing its high-q Fourier components and therefore the relaxation rate.

To apply this two-level transition rate to the multilevel situations in a relaxation cascade, one should use the total rate from the ith level to all the others, $w_i^* = \sum_f w_{if}$. But when the level neighboring the ith one is separated by more than E^{crit}, it is very likely that it achieves the only significant contribution to w_i^*, due to the very steep $w_{if} \propto E_{if}^{-5}$ relationship. Hence the separation between neighboring levels is needed to describe the reduced relaxation regime properly. Except for the unique case of the perfect parabolic well, the separation between neighboring levels is a quite distributed quantity (see Ref. 5 for examples). To deal with this aspect, we evidence in the next section a statistical distribution of these separations with a broad range of validity. We concentrate on the largest separations which are shown to limit electron relaxation.

Before going into this aspect, a safe check of Eq. (13) can be made with respect to the infinite 2DEG limit (i.e., large box size) where many final states significantly contribute to $w_i^* = \sum_f w_{if}$. In Appendix D, we show a simple way to achieve the final state summation, thus reconciling the L_x^{-4} behavior of w_{if} when $L_x \to \infty$ with the

classical L_x-independent 2DEG results.[16] It is thus seen that w_i^* is well suited to describe evolution from the infinite 2DEG regime to the reduced relaxation regime in a QB. This total rate is further discussed in the next section.

IV. STATISTICAL APPROACH AND BOTTLENECKS

The simplest way to get an order-of-magnitude calculation for relaxation in a multilevel quantum box in the $n=1$ case makes use of the average level separation $E_{\rm av}=g^{-1}$, g being the energy-independent density of states of a 2DEG. As shown in Appendix E, $E_{\rm av}$ is of the same order as the lateral confinement energy $E_{\rm conf}$ (i.e., $\pi^2\hbar^2/2m^*L_x^2$), familiar to practitioners in the field, namely, $E_{\rm av}=(4/\pi)E_{\rm conf}$. $E_{\rm conf}$ was indeed compared in Sec. II C to the threshold energy $E^{\rm crit}$ for reduced relaxation to get the order of magnitude of the threshold lateral size $L_x^{\rm crit}$ for reduced relaxation.

But separations $\Delta E=E_{if}$ significantly larger than $E_{\rm av}$ (and $E_{\rm conf}$) obviously exist between neighboring states in the cascade and act as bottlenecks, since their rate, w_{if} are the smallest. To quantify these separations, we introduce a reduced energy

$$u=E_{if}/E_{\rm conf}=(l^2+m^2)-(l'^2+m'^2)$$

for a square box ($u=4/\pi$ for $E_{if}=E_{\rm av}$). The critical value $L_x^{\rm crit}$ at which a given level pair separation $E_{if}=uE_{\rm conf}$ reaches $E^{\rm crit}$ depends on the particular pair chosen through u. From $E_{\rm conf}\propto L_x^{-2}$, it follows that $L_x^{\rm crit}\propto u^{1/2}$. For example, in Ref. 4 [$i=(2,1)$ and $f=(1,1)$], $u=3$ yields $L_x^{\rm crit}\approx 160$ nm, whereas the higher values $u\sim 6$ from the more realistic model of Ref. 5 yield $L_x^{\rm crit}\approx 230$ nm. To get more generality in this respect, we introduce in Sec. IV A a statistical approach, developed for the largest separations in Sec. IV B, and we focus on averaged transition rates and their significance in Sec. IV C.

A. The Poissonian distribution of separations

We show in Appendix E that the distribution of ΔE between neighboring levels of a finite 2DEG (and consequently of flat boxes) obeys a Poisson law of the form $p(\Delta E)=E_{\rm av}^{-1}\exp(-\Delta E/E_{\rm av})$ with not stringent assumptions, which make it relevant to boxes with quite arbitrary shapes, different from the square box. Going to rectangular boxes of high aspect ratio (pseudowires) would, however, require a different treatment. The case of a perfect parabolic well with separations $\Delta E=n\hbar\omega_0$ does not obey this Poisson law either, but it is quite unique in many respects. For the *exact* square box, two minor adaptations of this law are also needed, as discussed in Appendix E: (i) how to lift its accidental twofold degeneracy and (ii) why $E_{\rm av}$ is slightly increased above $(4/\pi)E_{\rm conf}$ when very few of the lower levels are considered, an adaptation which links to nonstatistical calculation.

As explained above, we focus on levels within one optical phonon energy ($E_{\rm opt}\approx 30$ meV) from the ground state. The number of such levels is $N=gE_{\rm opt}=E_{\rm opt}/E_{\rm av}\propto L_x^2$. Neglecting a correction of order $1/N$, we assume N to be also the number of separations. Relaxation properties are governed by those separations which exceed the threshold energy $E^{\rm crit}$ and how much they do so. The statistics of the ith smallest separation (counted from the smallest) and its expectation value E_i are detailed in Appendix E. We will show that the Nth largest separation E_N dominates bottlenecking effects.

B. Bottlenecks in a single subband

The essential result of Appendix E is that the average (expectation) value E_N of the largest of N separations is given by

$$E_N/E_{\rm v}=(1+\tfrac{1}{2}+\tfrac{1}{3}+\cdots+1/N)\approx(\ln N+C)$$

for large N ($C=0.577\ldots$ is Euler's constant). Thus, if N is large, E_N is significantly larger than $E_{\rm av}$. For example, for $N=150$ corresponding to $L_x\approx 240$ nm, $E_N/E_{\rm av}\approx 5.6$, a large value indeed. The average separation is then as low as $E_{\rm av}=E_{\rm opt}/N\approx 0.2$ meV, but still $E_N\approx 1.1$ meV lies in the vanishing relaxation regime. Thus bottlenecking phenomena can occur for $E_{\rm av}$ as low as 0.2 meV, that is, $E_{\rm conf}\approx 0.15$ meV. We find in particular that E_N is considerably larger than the separation $\Delta E=3E_{\rm conf}\approx 2.36E_{\rm av}$ used in Ref. 4. In terms of threshold size, these higher $E_N/E_{\rm av}$ values mean smaller $E_{\rm av}$ values to reach $E_N=E^{\rm crit}$, and thus larger threshold box sizes $L_x^{\rm crit}$ by a factor >1.5 to reach the reduced relaxation regime.

To get the N transition rates $\{w_i\}$ between neighboring levels, a first approach (to be refined in the next subsection) is to inject separation expectation values $\{E_i\}_{i=1\cdots N}$ into Eq. (13), using $q_{if}=E_{if}/\hbar c_s$. The slowest, bottlenecking, transition rate is of course w_N and it determines threshold size and overall evolution of bottlenecking phenomena. Notice, however, that, if E_N were not to play its role as a bottleneck due to some incidental peculiarity in the cascade E_{N-1} is close enough to E_N to act so for a close L_x value (the E_i's scale like L_x^{-2}). Hence the onset of bottlenecking phenomena is well defined in terms of lateral size.

However, there is no analytical expression in the statistical framework for the value $L_x^{\rm crit}$ of this onset: equating E_N and $E^{\rm crit}$ gives the following Eq. (14) of the form $\ln N=aN+b$:

$$E_N=(\ln N+C)E_{\rm av}=E_{\rm opt}(\ln N+C)/N$$
$$=E^{\rm crit}=\hbar c_s K_z=3hc_s/4L_z\ . \quad (14)$$

Let us recall that L_x and N are not independent: N being the number of levels below $E_{\rm opt}$ is essentially proportional to L_x^2. It is interesting, however, to write $L_x^{\rm crit}$ using only $\ln(N)$ (and not N) to compare to Eq. (4):

$$L_x^{\rm crit}\approx\left[\frac{\pi\hbar^2L_z(\ln N+C)}{3m^*c_s}\right]^{1/2}. \quad (15)$$

To discuss the evolution of w_N in the vanishing regime of Fig. 1(c) we make use of

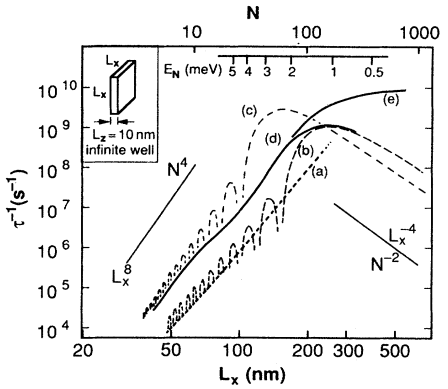

FIG. 2. Log-log plot of averaged transition rate (full lines) and other transition rates (dashed lines) in a square box with N levels under $E_{opt} \approx 30$ meV, the optical-phonon energy, as a function of L_x or $N \propto L_x^2$, in the infinite well limit. Curve *a*, small-N simplified behavior of Eq. (15); curve *b*, rate using the expectation value $(\ln N + C)E_{av}$ of the bottlenecking separation; curve *c*, rate using the two first (1,1) and (1,2) levels as in Ref. 6; curve *d*, averaged rate w_N at the bottleneck; curve *e*, average of summed rate to all lower-lying levels at the bottleneck w_N^*.

$$q \propto E_N \propto (\ln N + C)E_{av} = (\ln N + C)N^{-1}E_{opt} \ .$$

One finds, injecting $M_z(q) \propto q^{-6}$ (see Appendix C) and q in Eq. (13),

$$w_N \propto qM_z L_x^{-2} \propto q^{-5}L_x^{-2} \propto L_x^8[\ln(L_x^2)+C]^{-5}$$
$$\propto N^4(\ln N + C)^{-5} \ . \qquad (16)$$

The behavior of w_N is illustrated on curves *a* and *b* of Fig. 2 as a function of L_x for an $In_{0.53}Ga_{0.47}As$ box based on an $L_z = 10$ nm well and assuming infinite barriers. Parameters used in the calculations[17] are in Table I. Curve *a* (bold dashed line) represents the simplest approximation to Eq. (16) for w_N in the vanishing regime, first replacing $M_z(q)$ by its asymptotic $\pi^4[\sin^2(qL_z/2)](qL_z/2)^{-6}$ form (see Appendix C) and next averaging the oscillating factor to $\frac{1}{2}$, a helpful way to visualize asymptotic behavior. When N is large, the N^4 (i.e., L_x^8) power law dominates w_N behavior. When fewer levels are considered, the effective N exponent (slope of $\ln w_N$ vs N) departs below 4 because the $\ln N$ variation is no longer negligible (this deviation from N^4 is partly compensated by the low-N correction to E_{av} detailed in Appendix E). Curve *b* (thin dashed line) of Fig. 2 represents the exact w_N, well matching curve *a* below $L_x \sim 160$ nm. For larger L_x values, the behavior of M_z at lower q shows up, particularly in the abrupt drop around 200 nm. The L_x^{crit} value [Eq. (15)] is about 250 nm here, corresponding to $E_N \sim 1$ meV. The interest of the statistical approach can be seen by comparing curves *a* and *b* with curve *c*, where we only consider a two-level model between the ground and first excited states $(l,m)=(1,2)$ and (1,1) (meaning just that $u = E_{if}/E_{conf} = 3$ as in Ref. 4) restoring an exact L_x^8 envelope in the small-L_x limit [multiplied by $\sin^2(qL_z/2)$]. It is seen to give a lower ~ 150 nm threshold size whereas for this range $E_N \sim 2-3$ meV is more than twice as large as E^{crit}.

Another important conclusion which stems from Eq. (16) concerns the respective strength of the possibly numerous bottlenecks: the largest (Nth) separation dominates all the others even though E_{N-1} [$\approx (\ln N + C - 1)E_{av}$, cf. Appendix E] is not much smaller than E_N because $w_{if} \propto E_{if}^{-5}$, an exponent large enough to ensure that $w_{N-1} \gg w_N$ for the $N < 1000$ values we deal with.

C. Averaged bottlenecking rate

Experimentally evidencing the value of W_N as plotted above, including oscillations, is meaningless because, the approach being statistical, any particular realization will exhibit a scattering rate differing from the average by some *sizable* amount. We can preserve the virtues of our approach by applying it to an ensemble of boxes, a more realistic and feasible situation. It is easy to predict how the E_N's of such an ensemble are distributed from the law $p_N(E)$ (see Fig. 8 in Appendix E). They are seen to spread significantly around their average. In actual systems, such sizable changes between given levels $(l,m),(l',m')$ can originate from quite minor size or shape variations. It is indeed certain that a change of only a few percent in the box aspect ratio changes the actual bottleneck pair level. Another possible effect of such box-to-box variations could be to change N itself. In our statistical framework, the absolute value of the Nth level fluctuates by $N^{-1/2}$ in relative terms, being the sum of N Poissonian variables. Such a fluctuation has only a minute effect on the characteristic $\ln(N)$ factor for the largest separation. As for the other expressions where powers of N appear, they just stand for powers of L_x or better L_x^2, the box surface which gives the basic scaling of level separations. We want to account for fluctuations in box level separation which can occur at *constant* box surface and large lateral quantum numbers. This is the case when superimposing a weak random potential to the perfect box one: only the box shape is affected at first order,

TABLE I. Material parameters used in the calculation.

Parameter	Symbol	$In_{0.53}Ga_{0.47}As$	GaAs	Units
Effective mass	m^*	$0.0412m_0$	$0.067m_0$	m_0 is the free-electron mass
Sound velocity	c_s	3400	5150	$m\,s^{-1}$
Optical-phonon energy	E_{opt}	30	36	meV
Density	ρ	5500	5360	$kg\,m^{-3}$
Deformation potential	D	7.2	6.8	eV

and through the shape the largest separations. Changes in area and confinement are of second order. It is thus consistent to average w_N against $p_N(E)$, but not against N itself.

We thus claim that a physical measurement on an ensemble of boxes involves

$$w_N^{\rm av} = \int_0^\infty w(E) p_N(E) dE \tag{17}$$

rather than $w_N = w(E_N)$. In other words, the rate average has more physical significance than the rate at average bottleneck energy, $w[\int p_N(E) E\, dE]$. Using the rate average, we also wash out w_N's rapid oscillations which stem from M_z and could not be measured on an ensemble. This is because $E_{\rm av}$, the distribution characteristic width, covers many oscillations when $E_{\rm av} \gg E^{\rm crit}$.

As for departure from the infinite 2DEG limit ($E_N \sim E^{\rm crit}$, the drop leading to the first zero of M_z), it fortunately corresponds to $E_{\rm av}$ being only a fraction of $E^{\rm crit}$, so that the abrupt drop in M_z between the main maximum ($q=0$, $M_z=1$) and the secondary one ($q=5k_z$, $M_z < 10^{-3}$) is preserved in this average. On Fig. 2, curve d is the averaged rate $w_N^{\rm av}$ from the bottleneck level to its first lower-lying neighbor, at 0 K, for the same 10-nm-thick $In_{0.53}Ga_{0.47}As$ box with *infinite barriers*. It coincides with w_N (curve b) at large N, but significantly exceeds it at low N. This is due to the contribution of the distribution's low-energy tail, where rates proportional to E^{-5} considerably increase and compensate the small weight of $p_N(E)$ in $w_N^{\rm av}$.

One more step to go continuously from the 2DEG to the box case stems from the *number of final levels* accessible from a given level: the number of significant final levels for scattering in the 2DEG limit is roughly the *large* number of levels within $E^{\rm crit}$, and reduces to a *single* level in the bottlenecking limit. Thus the meaningful quantity describing energy relaxation from the 2DEG limit to the small-box limit is the scattering rate from level i to all final levels f, denoted $w_N^{\rm av*}$ and named hereafter the total rate.

To calculate this total rate $w_N^{\rm av*}$, one has to sum first $w(E)p_N(E)$ for the bottleneck itself, plus $w(E+E_{\rm av})p_N(E)$ for scattering to the next lower-lying level because it lies on the average $E_{\rm av}$ below the previous level, plus $w(E+2E_{\rm av})p_N(E)$ for the second neighbor, and so on, yielding

$$w_N^{\rm av*} = \int_0^\infty \left[\sum_{j=0}^{\infty} w(E + jE_{\rm av}) \right] p_N(E) dE \ . \tag{18}$$

We expect $w_N^{\rm av*}$ to stick to $w_N^{\rm av}$ for small boxes where the second neighbor $w(E+E_{\rm av}) \gg w(E)$ around $E = E_N$. Conversely, in the infinite 2DEG limit, many levels with comparable rates are summed, simply resulting in the well-known 2DEG acoustic scattering rate (see Appendix D).

On Fig. 2, curve e corresponds to the averaged total rate $w_N^{\rm av*}$ from bottleneck level to all lower-lying levels, which, unlike curves a–d, tends at large L_x towards the infinite 2DEG limit [Eq. (D3) in Appendix D]. Curves e and d exhibit a steep portion between $L_x \approx 100$ and 200 nm, with an effective exponent close to L_x^8, just after reduced relaxation onset. This preservation of a steep drop in spite of the averaging procedure further justifies the idea of a threshold for reduced relaxation.

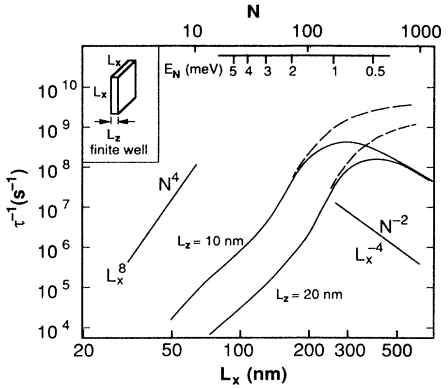

FIG. 3. Log-log plot of the averaged bottlenecking rates w_N and w_N^* (sum on all final states) as a function of L_x or $N \propto L_x^2$, for a finite well of $In_{0.47}Ga_{0.53}As$ lattice-matched to InP of thickness $L_z = 10$ and 20 nm.

Going to finite barriers has, in the $In_{0.53}Ga_{0.47}As/InP$ system, little effect on $w_N^{\rm av}$ and $w_N^{\rm av*}$ for $L_z = 10$ nm, as shown in Fig. 3. For $L_z = 20$ nm, the curves shift more clearly to still larger lateral dimensions. Thresholds $L_x^{\rm crit}$ are 300 nm for $L_z = 10$ nm and 420 nm for $L_z = 20$ nm. The 300 nm $L_x^{\rm crit}$ value, larger than its infinite-well counterpart (Fig. 2), is connected with the lower k_w wave vector in the well due to barrier finiteness. Both curves are seen to be similar, except for the higher threshold value of the wider 20 nm well.

The detailed dependence of this threshold value $L_x^{\rm crit}$ for reduced relaxation as a function of initial well thickness L_z is plotted on Fig. 4 for (curve a) the $In_{0.53}Ga_{0.47}As/InP$ system and (curve b) the

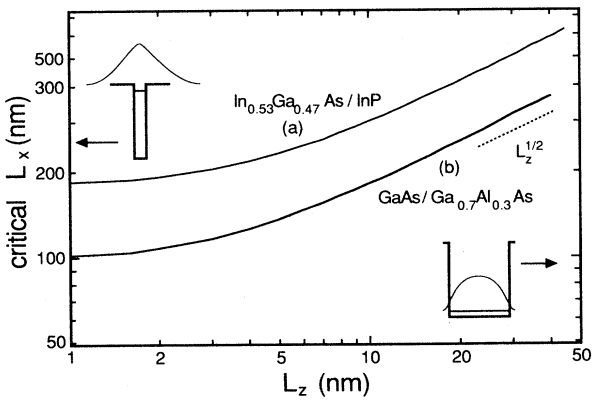

FIG. 4. Log-log plot of the critical value $L_x^{\rm crit}$ for reduced relaxation as a function of the thickness L_z of the initial well, for (curve a) the $In_{0.53}Ga_{0.47}As/InP$ system; (curve b) the $GaAs/Ga_{0.7}Al_{0.3}As$ system. The asymptotic trends are like $L_z^{-1/2}$ for large L_z and determined by the mere barrier height for the infinitely narrow well. The z wave function and band profile are schematized in both limits.

GaAs/$Ga_{0.7}Al_{0.3}As$ system. It is determined by Eq. (14), equating the largest L_x-dependent separation E_N to the L_z-dependent threshold separation for reduced relaxation $E^{crit}=\hbar c_s K_z$. Barrier finiteness is most felt at low L_z where K_z saturates at the value k_B determined by the conduction-band offset $\Delta E_c=\hbar^2 k_b^2/2m^*$, the $n=1$ level reaching the barrier top. Conversely, the large-L_z limit yields $L_x^{crit}\propto L_z^{1/2}$ as in Eqs. (4) and (15). This is responsible for the different shoulder locations in Fig. 3 by a factor $\approx(2)^{1/2}$. The $(\ln N+C)$ factor in E_N has little effect here. Notice the largest L_x values for the In-based material (curve *a*), following the $(m^*c_s)^{-1/2}$ scaling of Eq. (4). Here, the larger effective mass and sound velocity of GaAs determine an L_x^{crit} value smaller by a factor of ~ 1.6 than in $In_{0.53}Ga_{0.47}As$.

D. Bottlenecking and higher subbands

We present in Fig. 5 adaptations of averaged rates to the intersubband case, $i\equiv(l,m,2)$ and $f\equiv(l',m',2)$ or $f\equiv(l',m',1)$ for a large initial well $L_z=30$ nm patterned into boxes, still in the $In_{0.53}Ga_{0.47}As/InP$ system. In this well, $E_{n=2}-E_{n=1}\approx 25$ meV, an ideal value for infrared applications below the optical-phonon energy, namely, at 50 μm.[11] As for the validity of such calculations, which violate the initial $q_\parallel \ll q_z$ assumption, we checked numerically on Eq. (9) that, in the second subband bottom where these rates are relevant, the dominant contribution still comes from the poles of the depicted q sphere, making Eq. (13) still valid. The 2-2 transition has a smaller threshold size than the 2-1, and this latter is still smaller than the 1-1 of the same well, due to larger momentum and larger phonon energies available through higher K_z in $n=2$ subband states. The 2-1 level-to-level transition rate decreases faster than L_x^{-4} at large L_x because $M_z^{2,1}$ vanishes at $q=0$. The 2-2 rate does not vanish at $q=0$ but at $q=2\pi/L_z$ before its noticeable secondary maximum, and this is preserved through the averaging procedure.

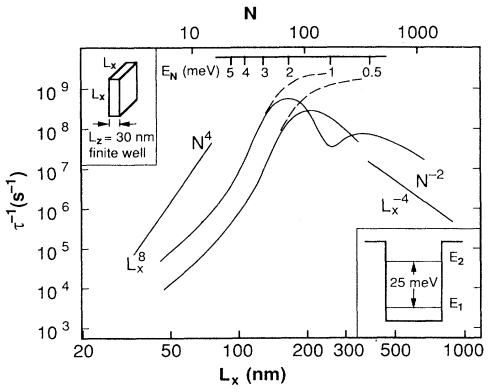

FIG. 5. Log-log plot of the averaged bottlenecking rates w_N and w_N^* as a function of L_x or $N\propto L_x^2$, from the $n=2$ pseudosubband of a finite well of $In_{0.53}Ga_{0.47}As$ lattice-matched to InP of thickness $L_z=30$ nm to the $n=1$ pseudosubband (intersubband) (curve without dip) and the $n=2$ pseudosubband (intrasubband) (curve with a dip at 250 nm).

Finally, the essential features of reduced relaxation found in the first subband should hold for higher subbands, still in *n*-doped semiconductors, provided the absolute energy remains below quantized excitations such as optical phonons. It is not the aim of this paper to describe the many complex phenomena arising far from conduction-band minima, such as nonparabolicity, etc. Similarly, if some very-low-energy excitations (e.g., localized phonons, . . .) interact with carriers, due to impurities at surfaces, an additional relaxation channel appears. Our discussion should, however, hold for properly buried quantum boxes with clean interfaces and acoustic phonons very close to bulk ones. The essential point to retain is that for moderate confinements relaxation through a level cascade may be reduced more than calculated by, e.g., Ref. 4, because, as quantified in the statistical approach, level separations significantly larger than the average show up in such cascades.

V. SUMMARY AND CONCLUSION

The electron–acoustic-phonon scattering rate between box levels has been calculated analytically, in particular for separations larger than $E^{crit}\approx 1$ meV where it vanishes rapidly, causing strongly reduced relaxation of electrons. Crucial to envisioned applications of boxes is this low value of E^{crit}, much lower than the usual criterion of leading to $a\sim 25$ meV separation necessary to get true 0D behavior at room temperature.

We developed a statistical approach to predict, among a cascade of N square-box levels situated under the optical phonon energy E_{opt}, the magnitude of the largest, bottlenecking, energy separation E_N. Expressed in the familiar units of E_{conf}, this magnitude $u=E_N/E_{conf}$ is of the order of $(4/\pi)(\ln N+0.58)$. It turns out to be significantly larger at the onset of reduced relaxation than the value $u=3$ used in Ref. 4. This is because a confinement energy of 0.16 meV and an average separation of 0.2 meV (i.e., $N\sim 150$), making u of the order of ~ 7, allows reaching the $E^{crit}\approx 1$ meV threshold separation in examples studied here.

Furthermore, statistics yield averaged rates w_N and w_N^* with a true physical meaning for an ensemble of QB's. These rates exhibit a well-defined threshold size L_x^{crit} for reduced relaxation, of the order of 250 nm for a typical 10 nm $In_{0.47}Ga_{0.53}As/InP$ well. The behavior of these rates for L_x just below L_x^{crit} is as steep as L_x^8 or N^4. For smaller sizes, Eq. (16) yields a slightly smaller effective exponent.

The statistics also allows us to tell that the number of bottlenecks in the cascade increases rapidly when sizes are decreased below L_x^{crit}. The exact location of the first or the second bottleneck along the cascade is therefore not crucial: for a small change in size, another bottleneck comes in, and sooner or later the crucial part of the cascade undergoes reduced relaxation. This means that the threshold L_x^{crit} is effective in predicting relaxation properties of the whole cascade.

Still, we predict that, bottlenecks being in series, the strongest of them dominates the overall behavior, due to the steep behavior of $M_z(q)\propto q^{-6}$. Therefore not only

the threshold size but also the vanishing behavior of $w_N^{\rm av}$ do describe the cascade relaxation properties under $E_{\rm opt}$.

Extensions of these results to the two intersubband cases (1,2) and (2,2) in the z direction have also been presented with similar conclusions.[11]

Finally, we have considered so far acoustic phonons and neglected LO phonons, mostly focusing on energies lower than $E_{\rm opt}$. But it can be seen that our predictions are essentially valid for acoustic phonons if z-subband indices are reasonably low. At low temperatures especially, multiphonon processes are expected to be weak. Then monochromaticity of LO phonons allows for a typical ~ 1 meV spreading around $E_{\rm opt}$ to induce a transition rate >1 ns^{-1} between electronic levels. Therefore, when $E_{\rm av}$ becomes larger than 1 meV, presumably in the 2–5 meV range, the probability of LO transitions should decrease extremely steeply, falling even below acoustic-phonon rates. Therefore, except for a moderate reduction of the threshold size $L_x^{\rm crit}$ and a steeper behavior around this size, the low-size tail of the results presented here still retains its significance for the whole energy range as a first-order result, of interest for infrared devices.[11]

ACKNOWLEDGMENTS

This work has been partly supported by ESPRIT No. 3133 "NANSDEV." The author would like to thank C. Weisbuch for invaluable discussions and critical reading of the manuscript, and also B. Vinter, J. Pian, and M. Kanehisa for useful discussions.

APPENDIX A: THE ONE-DIMENSIONAL MATRIX ELEMENT BETWEEN l and l' ENVELOPE WAVE FUNCTIONS

Taking the origin at midwell, envelopes are of the form $\cos(l\pi/L_x)$ for l odd and $\sin(l\pi/L_x)$ for l even. From the products of l and l' envelopes, one has the signs of Table II for the coefficient of $\exp\{i[(\pm l\pm l')\pi/L_x+q]x\}$, which turn out to be the factors s_ν of Eq. (4).

APPENDIX B: q summation of M_x

Dropping x indices and using $Q=qL/2$ and the reduced length $u=2x/L$, the matrix element $M_x(q)$, for example, in the case of l and l' both odd, can be written as a Q Fourier transform

$$\langle l|\exp(iqx)|l'\rangle = \int_{-1}^{1}\cos(l\pi u/2)\cos(l'\pi u/2)\exp(iQu)du \ . \quad \text{(B1)}$$

Hence, turning to the squared matrix element $M(q)$, we have

$$\int M(Q)dQ=\frac{L}{2}\int M(q)dq = \int dQ|\mathsf{F}\{\cos(l\pi u/2)\cos(l'\pi u/2) \times\theta(1-u)\theta(1+u)\}|^2 \ , \quad \text{(B2)}$$

where F is the Fourier transform and θ the usual Heaviside step function $[\theta(x<0)=1,\theta(x>0)=0]$. Then the Bessel-Parseval theorem tell us that this latter sum is also the sum of the squared initial function:

$$\frac{L}{2}\int M(q)dq=(2\pi)\int_{-1}^{1}\cos^2(l\pi u/2)\cos^2(l'\pi u/2)du \ . \quad \text{(B3)}$$

Thus we have, generalizing to any envelope (cos or sin) and using classical properties of sin and cos functions,

$$\frac{L}{2}\int M(q)dq=(2\pi)\int_{-1}^{1}[\tfrac{1}{2}\pm\tfrac{1}{2}\cos(l\pi u)] \times[\tfrac{1}{2}\pm\tfrac{1}{2}\cos(l'\pi u)]du =(2\pi)(\tfrac{1}{2}+\tfrac{1}{4}\delta_{ll'}) \ , \quad \text{(B4)}$$

which amounts to Eq. (11) of the text.

APPENDIX C: LARGE-q BEHAVIOR OF M_z

For the $n=n'=1$ case, we have, with $Q=q_2L_z/2$,

$$M_z=\left|\frac{\sin(Q)}{Q}+\frac{\sin(Q+\pi)}{2(Q+\pi)}+\frac{\sin(Q-\pi)}{2(Q-\pi)}\right|^2 =\sin^2Q\left|\frac{\pi^2}{Q(Q^2-\pi^2)}\right|^2 . \quad \text{(C1)}$$

Since $Q\propto q_{if}\propto L_x^{-2}$, when $Q\gg\pi$, we have, averaging the $\sin^2Q$ factor to $\frac{1}{2}$,

$$M_z=\frac{\pi^4\sin^2Q}{2Q^6}\sim L_x^{12} \ . \quad \text{(C2)}$$

This behavior also holds for a finite well because the wave function is smoother in such a well, which means lower high-spatial-frequency amplitudes in the Fourier transform $M_z(q)$.

APPENDIX D: SCATTERING RATES AND ENERGY-LOSS RATES FOR LEVELS IN THE LARGE-SQUARE-BOX LIMIT

We calculate here the scattering rate $w_i^*=\sum_f w_{if}$ from one level i to all the others f, in the very-large-L_x case $E_{\rm av}\ll E^{\rm crit}$ (~ 1 meV in our system). We use the average separation $E_{\rm av}=g^{-1}$, where g is the density of state; of

TABLE II. Coefficients of the $\pm l\pm l'$ terms in the matrix element M_x.

Case		Type of envelope		Coefficient s_ν			
l	l'	l	l'	$(l+l')$	$-(l+l')$	$l'-l$	$l-l'$
odd	odd	cos	cos	1	1	1	1
odd	even	cos	sin	1	−1	1	−1
even	even	sin	sin	1	1	−1	−1

the same order as the confinement energy $E_{\rm conf}$ [$E_{\rm av}=(4/\pi)E_{\rm conf}$, see Appendix E].

The matrix element M_z is of order unity only for the $N_r=E^{\rm crit}/E_{\rm av}$ levels $|f\rangle$ on each side of $|i\rangle$ which consequently achieve the main contribution to w_i^*. This infinite-2DEG limit amounts to Kawaji's[16] classical result for elastic scattering of electrons by phonons. In fact, scattered electrons do suffer small but nonzero energy change because, due to the finite extent of Ψ_z, phonons can take momentum from electrons up to $\sim h/L_z$ and energy up to $E^{\rm crit}$.

If one is in the equipartition regime for phonons (high temperature), then $n_B\approx n_B'\approx k_BT/\hbar c_s q_{if}$ in Eq. (13). Consequently, the $2N_r$ levels $|f\rangle$ lying within $E^{\rm crit}$ of $|i\rangle$ have the same $E_{\rm if}$-independent scattering rate w_{if},

$$w_{if}=\frac{D^2}{\rho\hbar^2c_s^3}\frac{k_BT}{L_x^2}\ , \tag{D1}$$

since $M_z\sim 1$ ($l\neq l'$ and $m\neq m'$ for a general case). Multiplying by $2N_r$ gives

$$w_i^*\approx 2w_{if}\frac{E^{\rm crit}}{E_{\rm av}}=\frac{3m^*k_BTD^2}{2\rho\hbar^3c_s^2L_z}\ , \tag{D2}$$

which is Kawaji's result.[16]

At low temperature where $n_B\ll 1$ and $n_B'\approx 1$, $w_{if}\propto q_{if}$ and thus $w_{if}\propto E_{if}$. Then averaging E_{if} over the N_r levels yields $E^{\rm crit}/2$ and a size-independent rate w_i^* is again found,

$$w_i^*\approx\frac{9\pi m^*D^2}{4\rho\hbar^2c_sL_z^2}\ , \tag{D3}$$

still in the usual nanosecond range.

Therefore Eq. (13) and its L_x^{-4} factor are reconciled with the infinite 2DEG. Also energy-loss rates obtained by weighting w_{if} with E_{if} before summing on $|f\rangle$ levels are L_x independent when $E_{\rm av}\ll E^{\rm crit}$. No difference between the high- and low-temperature regimes is needed because, if all the final levels surrounding the initial level are assumed to have the same zero occupancy, the balance between phonon emission and absorption at a given E_{if} is $(n_B'-n_B)E_{if}=E_{if}$, independent of the temperature. In the $w_{if}E_{if}$ product, a factor E_{if}^2 appears, whose expectation value in the $[0,E^{\rm crit}]$ interval is now $[(E^{\rm crit})^2]/3$. Multiplying by N_r gives

$$\frac{\partial E}{\partial t}=\frac{9\pi^2m^*D^2}{8\rho\hbar L_z^3}\ . \tag{D4}$$

APPENDIX E: STATISTICS OF THE LEVEL SEPARATION IN A GIVEN SUBBAND OF A BOX

Unlike the case of a continuum, relaxation studies in realistic quantum boxes have to take into account the detailed distribution of level separations. It is most instructive to introduce the basic concepts dealt with here from an example. Figure 6 shows a histogram of the level separations in a square box with infinite barriers, in the first subband ($n=1$ set), for (a) the $N=1500$, (b) the $N=160$, (c) the $N=14$ lower levels. It is expressed in reduced units of the average level separation $x=E/E_{\rm av}$. $E_{\rm av}$ is just the inverse 2D energy-independent density of states $E_{\rm av}=g^{-1}=(4/\pi)E_{\rm conf}$ as will be seen below. The box is actually slightly rectangular (by a few percent at most) keeping the L_xL_y area constant, in order to lift the accidental twofold degeneracy of the perfect square box $E_{l,m}=E_{m,l}$.

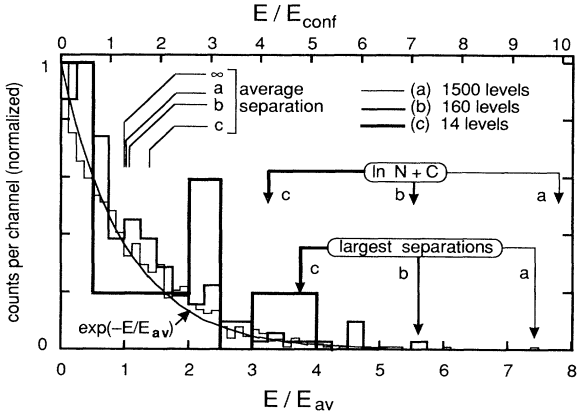

FIG. 6. Histograms of the separation distribution in a square box (first z subband) for the first N levels as a function of $x=E/E_{\rm av}$ (bottom) or $E/E_{\rm conf}=(\pi/4)x$ (top), compared with the $\exp(-x)$ Poissonian law (solid curve). (a) $N=1500$; (b) $N=160$; (c) $N=14$. Arrows outline the largest separation in each case, scaling like $x=\ln N$. The average separation shifts slightly but significantly above the $x=1$ ($N=\infty$) value as N vanishes.

The main features that appear are the following. (i) The Poissonian distribution of the separations $p(x)=\exp(-x)$, as indicated by the dashed curve. (ii) The largest separations $x_{\rm max}$ of each distribution, outlined by an arrow, which are in the (c) < (b) < (a) order. The correlation with $x=\ln 1500$ (a), $\ln 160$ (b), and $\ln 30$ (c) (see the figure) suggests that $x_{\rm max}$ scales like $\ln N$. (iii) Looking more carefully, the (b) and (c) histograms decay more slowly than $\exp(-x)$. This due to a small but nonnegligible increase of the actual average separation above g^{-1} for small N values, as indicated on the figure and as will be explained below from the way the levels fill the k space. In the next subsections, a theoretical basis is given for the above features, aiming to introduce finally the distribution law of the largest of N separations.

1. Poissonian distribution of level separations

Let us consider a collection of N levels uniformly distributed on a $[0,E_{\rm opt}]$ interval. Physically, levels in this interval cannot undergo scattering by optical phonons. The uniform energy distribution corresponds to the classical energy-independent density of states of a 2DEG within a single subband and assuming a parabolic dispersion relation. The density of probability to find a level between E and $E+dE$ is thus

$$(dp_0/dE)=N/E_{\rm opt}=g=1/E_{\rm av}\ , \tag{E1}$$

where $E_{\rm av}$ is the average energy separation and g ($\equiv g_{\rm 2D}$) the (energy-independent) density of states. To get the separation distribution between two neighbor levels, we assume that there is a level at a given energy. Then, the probability $p_1(E+dE)$ that the separation is larger than $E+dE$ is the product of the probability $p_1(E)$ that the separation is larger than E by the probability $(1-g\,dE)$ that there is no level between E and $E+dE$. Thus

$$p_1(E+dE)=p_1(E)(1-g\,dE) \tag{E2}$$

and therefore

$$dp_1(E)/dE=-gp_1(E),\quad p_1(E)=\exp(-gE)\ , \tag{E3}$$

where $p_1(E=0)=1$ is achieved. The distribution law p of the separation is hence

$$p(E)=-dp_1(E)/dE=g\exp(-gE)\ , \tag{E4}$$

which is a Poissonian law.

2. The case of the rectangular box

In a square box of side L, if we do not consider spin degeneracy, we have in the large-N limit

$$g=\frac{2m^*}{\hbar^2}\frac{L^2}{4\pi},\quad E_{\rm av}=\frac{4}{\pi}\frac{\hbar^2}{2m^*}\frac{\pi^2}{L^2}\ . \tag{E5}$$

For this particular case, the Poissonian law was well verified above, lifting, however, the accidental twofold degeneracy ($E_{l,m}=E_{m,l}$).

In the low-N limit, the average separation $E_{\rm av}$ is found to be systematically above the value of Eq. (E5) above, the first factor ($4/\pi=1.27\ldots$) reaching about 2. The reason for this is made clear in Fig. 7 where the k_x-k_y plane is represented with the quantized k_x,k_y values in the box. The energy is proportional to k^2. Hence a circle arc corresponding to the $E_{\rm opt}$ limit has been drawn, the enclosed area A being proportional to $E_{\rm opt}$. In the large-N limit (larger arc), we recover the constant density of states because A is proportional to the number of levels N, each level corresponding to the same π^2/L^2 area. Let us examine more precisely the tiling of the plane by squares of this π^2/L^2 area on Fig. 7. This tiling covers only the $[\pi/2L,\infty[^2$ region. At low N (smaller arc), a noticeable portion of A lies outside the tiled region. This rarefies the density of levels and increases $E_{\rm av}$, up to a factor of about 1.7 for $N=4$, i.e., when only the first four levels (1,1) (1,2), (2,1), and (2,2) are considered. As can be guessed from the figure, the correction for the missing surface scales like the arc radius and therefore as $N^{1/2}$. A good approximation of $E_{\rm av}$ is more precisely given by

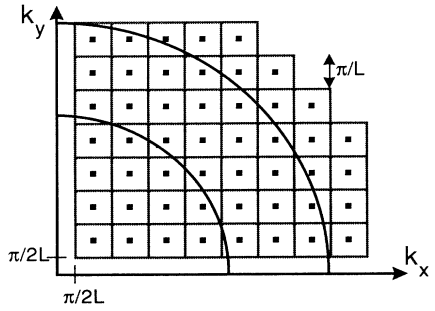

FIG. 7. Quantized k values $l\pi/L_x, m\pi/L_x$ of the square box levels in the $\mathbf{k}$ plane and the tiling by squares of area π^2/L_x^2.

$$E_{\rm av}\approx(E_{\rm av})_{N=\infty}\left[1+\frac{2}{\sqrt{\pi N}}\right]\ , \tag{E6}$$

which fortunately matches the $N=4$ case very well. We checked that this law is in good agreement with the actual average for a square box.

3. Statistics for an ordered collection of spacings

We consider a collection of N separations, each obeying independently the Poissonian law of Eq. (E4). Rigorously, one should take $N-1$ spacings for N levels, but this correction is of order $1/N$, not as large as the correction for low N in a square box above, of order $N^{-1/2}$. We assume that they are labeled in ascending order and write them $E_1<E_2<\cdots<E_i<\cdots<E_{N-1}<E_N$. We deduce the distribution law of the ith smallest separation from the Poissonian distribution of the separation as follows. If E_i has a given value E, which has the probability $p(E)$, then we need to have $(N-i)$ separations larger than E, whatever their order, and $(i-1)$ separations smaller than E, whatever their order. The first requirement is described by a $p_1(E)^{(N-i)}$ factor and the second by a $[1-p_1(E)]^{(i-1)}$ factor, so that the distribution law of the ith separation has the form

$$p_i(E)\propto p(E)p_1(E)^{(N-i)}[1-p_1(E)]^{(i-1)}\ . \tag{E7}$$

Since $p(E)=gp_1(E)$, we have the distribution law

$$p_i(E)=gi\begin{bmatrix}N\\ i\end{bmatrix}\exp(-gE)^{(N-i+1)}\times[1-\exp(-gE)]^{(i-1)}\ . \tag{E8}$$

The coefficient for normalization is found by iterative integration by parts of the probability product.

4. Properties of p_i

The reduced variable $x=gE$ will be used in the following, and we denote $j=N-i+l$: the ith smaller separation is the jth larger. The law $p_i(x)$ peaks for $\exp(-x_{\rm peak})=j/N$, $x_{\rm peak}=\ln N-\ln j$. It has an $\exp(-jx)$ behavior toward infinite x and an $(i-1)$ power-law behavior for vanishing x. It can be shown to have an expectation value

$$x_i=[1/N+1/(N-1)+1/(N-2)+\cdots+1/j]$$

from iterative integration by parts of $xp_i(x)$, using a primitive of $x\exp(-x)$ to decrease the exponent of $[1-\exp(-x)]$.

The x_i value can also be found with a heuristic argument. The N separations, with their Poissonian distribution law $\exp(-x)$, can be compared to N decaying parti-

cles of lifetime T. After a time T/N, on the average, one of the N particles has decayed, and $(N-1)$ are left. Then an average delay $T/(N-1)$ is needed for the second decay (decaying particles do not "age"), that is, a total time $T[1/N+1/(N-1)]$ from the beginning, and so on.

As for the variance of p_i, it can be estimated by looking at the inflection points of the distribution on each side of the peak, since the law is bell shaped. They are expressed as

$$x_{\text{infl}}=-\ln\left\{\frac{j}{N}+\frac{i-1}{2N^2}\left[1\pm\left[1+\frac{4jN}{i-1}\right]^{1/2}\right]\right\}. \quad \text{(E9)}$$

5. Approximation for the larger separations: large N, vanishing j/N

If N is very large, the above law is unpractical to handle. Since the law for the jth larger separation has a relatively narrow peak for vanishing j/N, a development around the peak can be made using $(1+a/n)^n\approx\exp(a)$ for large n, and gives the following result:

$$p_i(x)\approx\frac{i}{N^j}\begin{bmatrix}N\\ i\end{bmatrix}\exp(-jx')\exp[-\exp(-x')] \quad \text{(E10)}$$

with $x'=x-\ln N$. This law also peaks at $x'=-\ln j$ (that is, $x=\ln N-\ln j$). It has its inflections at

$$x'_{\text{infl}}=-\ln[j+\tfrac{1}{2}\pm\sqrt{j+\tfrac{1}{4}}]\,. \quad \text{(E11)}$$

For large j (but still with vanishing j/N), this law tends to a Gaussian of mean-square deviation $1/j$ (width $2/\sqrt{j}$).

6. Application to the bottlenecking relaxation rate: $p_N(x), j=1$

The largest out of the N separations has the law

$$p_N(x)=N\exp(-x)[1-\exp(-x)]^{(N-1)}\,, \quad \text{(E12)}$$

which is the derivative of the law

$$p_{1,N}(E)=[1-\exp(-x)]^N\,. \quad \text{(E13)}$$

From the above results, $p_N(x)$ peaks at $x_{\text{peak}}=\ln N$. Its inflection points in the large-N limit are given by

$$x_{\text{infl}}=\ln N-\ln\left[\frac{3\pm\sqrt{5}}{2}\right],\qquad x'_{\text{infl}}=-\ln\left[\frac{3\pm\sqrt{5}}{2}\right], \quad \text{(E14)}$$

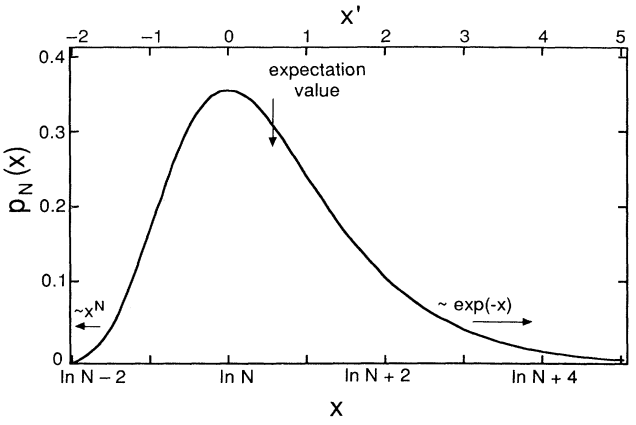

FIG. 8. Distribution law $p_N(x)$ of the largest out of N Poissonian separations, as a function of x or $x'=x-\ln N$, in the large-N limit. $p_N(x')=\exp(-x')(\exp\{-[\exp(-x')]\})$. The expectation value is $(\ln N+C)$ where $C=0.577\ldots$ is Euler's constant. Behaviors for $x\gg\ln N$ and $x\ll\ln N$ are indicated.

which gives the order of magnitude of the variance. As for the expectation value, it is exactly

$$x_N=1/N+1/(N-1)+1/(N-2)+\cdots+\tfrac{1}{2}+1\,. \quad \text{(E15)}$$

In the large-N limit, we therefore have $x_X\approx\ln N+C$ where $C=0.577\ldots$ is known as Euler's constant. This difference $x_N-x_{\text{peak}}=C$ reflects the contrasted behavior of p_N on each side of the peak: p_N has a relatively "slow" exponential decay at large x, whereas at small x it has a very abrupt exponential of exponential ["exp(exp)"] behavior. This is obvious if the approximation of Eq. (E10) is written in this particular case $j=1$, as a function of $x'=x-\ln N$:

$$p_N(x)=\exp(-x')\exp[-\exp(-x')]\,, \quad \text{(E16)}$$

which is the derivative of the function $\exp[-\exp(-x')]$. p_N is plotted on Fig. 8 as a function of x and x', in this large-N limit, recalling its main features: peak at $x=\ln N$, expectation value $(\ln N+C)$, asymmetric shape extending over a few units of x.

[1]Y. Arakawa and H. Sakaki, Appl. Phys. Lett. **24**, 195 (1982); Y. Arakawa, H. Sakaki, M. Nishioka, H. Okamoto, and N. Miura, Jpn. J. Appl. Phys. **22**, 804 (1983); Y. Arakawa and A. Yariv, IEEE J. Quantum Electron. **QE-22**, 1887 (1986).

[2]Y. Miyamoto, M. Asada, and Y. Suematsu, IEEE J. Quantum Electron. **QE-25**, 2001 (1989); M. Asada, Y. Miyamoto, and Y. Suematsu, Jpn. J. Appl. Phys. **24**, 95 (1985); S. Schmitt-Rink, D. A. B. Miller, and D. S. Chemla, Phys. Rev. B **38**, 6976 (1986).

[3]C. Weisbuch and J. Nagle, in *Science and Engineering of One- and Zero-Dimensional Semiconductors*, Vol. 214 of *NATO Advanced Study Institute, Series B: Physics*, edited by S. P. Beaumont and C. M. Sotomayor-Torres (Plenum, New York, 1990); C. Weisbuch and B. Vinter, *Quantum Semiconductor Structures* (Academic, Boston, 1991), Chaps. 3 and 6.

[4]U. Bockelmann and G. Bastard, Phys. Rev. B **42**, 8947 (1990).

[5]H. Benisty, C. M. Sotomayor-Torres, and C. Weisbuch, Phys. Rev. B **44**, 10 945 (1991).

[6]P. D. Wang, C. M. Sotomayor-Torres, H. McLelland, S. Thoms, M. Holland, and C. R. Stanley, Surf. Sci. **305**, 585

(1994).
[7]K. Brünner, U. Bockelmann, G. Abstreiter, M. Walther, G. Böhm, G. Tränkle, and G. Weimann, Phys. Rev. Lett. **69**, 3216 (1992).
[8]T. Inoshita and H. Sakaki, Phys. Rev. B **46**, 7260 (1992).
[9]U. Bockelmann and T. Egeler, Phys. Rev. B **46**, 15 574 (1992).
[10]U. Bockelmann, Phys. Rev. B **48**, 17 637 (1993).
[11]H. Benisty and C. Weisbuch (unpublished).
[12]L. Swierowski, W. Zawadzki, Y. Guldner, and C. Rigaux, Solid State Commun. **27**, 1245 (1978).
[13]R. Ferreira and G. Bastard, Phys. Rev. B **40**, 1074 (1989).
[14]Y. Okuyama and N. Tokuda, Phys. Rev. B **40**, 9744 (1989).
[15]G. Bastard, *Wave Mechanics Applied to Semiconductor Heterostructures* (Les Editions de Physique, Les Ulis, 1988).
[16]S. Kawaji, J. Phys. Soc. Jpn. **27**, 906 (1969).
[17]J. S. Blakemore, J. Appl. Phys. **53**, 123 (1982); see also Ref. 4.

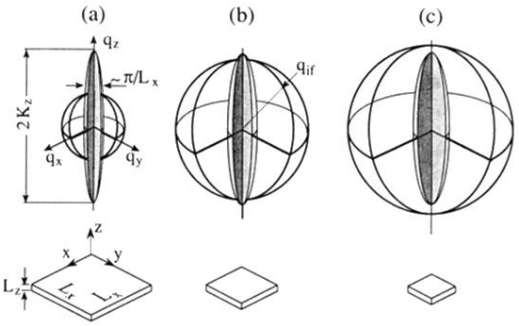

FIG. 1. Picture in the q space of the energy-conserving sphere of radius q_{if} and of the region of momentum conservation $M \sim 1$ for transition between levels of a square box of dimensions $L_x \times L_x \times L_z$. q_{if} scales like L_x^{-2} while the $q_\parallel$ extent of M scales like L_x^{-1} and the q_z extent is constant. (a) Large L_x: the $M \sim 1$ region intersects the sphere; (b) smaller L_x: intermediate case, $q_{if} \approx 3\pi/(2L_z)$; (c) small L_x: the sphere intersects only regions of vanishing M.